The Newton-Raphson method for solving non-linear and anisotropic time-harmonic problems

H. Vande Sande
Flanders' Mechatronics Technology Centre, Heverlee, Belgium
F. Henrotte and K. Hameyer
Rheinisch-Westfälische Technische Hochschule, Aachen (RWTH Aachen)
Institut für Elektrische Maschinen (IEM), Aachen, Germany

Keywords *Modelling, Magnetic fields, Newton-Raphson method*

Abstract *This paper discusses the use of a complex-valued reluctivity tensor for modelling non-linear, anisotropic and hysteretic materials in a time-harmonic finite element context. It is shown how these problems can be solved by the Newton-Raphson method. The method is applied for the simulation of the magnetic field distribution in a three-phase transformer.*

1. Time-harmonic finite element method

The time-harmonic finite element method allows to simulate the steady-state behaviour of devices that are excited by sinusoidally varying currents. The governing equation of a two-dimensional time-harmonic problem is

$$\nabla \cdot (\nu' \nabla \tilde{A}) - j\sigma\omega\tilde{A} = -\tilde{J}, \tag{1}$$

where

$$\nu' = \begin{pmatrix} \nu_{yy} & -\nu_{yx} \\ -\nu_{xy} & \nu_{xx} \end{pmatrix} \tag{2}$$

is a matrix containing the entries of the reluctivity tensor ν [Am/Vs], σ the electric conductivity [A/Vm], ω the pulsation frequency [rad/s], $\tilde{A}$ the z-component of the magnetic vector potential [Vs/m] and $\tilde{J}$ the z-component of the applied current sources [A/m^2]. $\tilde{A}$ and $\tilde{J}$ are phasors and are represented by complex numbers. The instantaneous value of the vector potential in time-domain is determined by

$$\vec{A}(t) = \Re\{\tilde{A}e^{j\omega t}\}. \tag{3}$$

The piecewise continuous approximation of the magnetic vector potential over the finite element mesh writes

$$\tilde{A}(x,y) = \sum_{i=1}^{n} \tilde{A}_i \varphi_i(x,y), \tag{4}$$

The authors are grateful to the Belgian "Fonds door Wetenschappelijk Onderzoek Vlaanderen" (project G.0427.98) and the Belgian Ministry of Scientific Research (IUAP No. P5/34).

COMPEL: The International Journal for Computation and Mathematics in Electrical and Electronic Engineering
Vol. 23 No. 4, 2004
pp. 950-958

0332-1649
DOI 10.1108/03321640410553373

where n is the number of nodes in the mesh and φ_i is the shape function in node i of the mesh. After applying the Galerkin approach, one finally ends up with a system of algebraic equations:

$$\tilde{\mathbf{r}}(\tilde{\mathbf{A}}) = (\mathbf{K}(\tilde{\mathbf{A}}) + j\mathbf{L})\tilde{\mathbf{A}} - \tilde{\mathbf{T}} = \mathbf{0}, \tag{5}$$

where $\tilde{\mathbf{A}}$ is the solution vector, $\tilde{\mathbf{T}}$ the source vector, $\tilde{\mathbf{r}}$ the residual vector, $\mathbf{K}$ the stiffness matrix and $\mathbf{L}$ the eddy-current matrix. The non-linearity of the problem is due to the dependency of $\mathbf{K}$ on $\tilde{\mathbf{A}}$, via the reluctivity tensor.

2. Reluctivity tensor

In a time-harmonic context, non-linear, anisotropic and hysteretic behaviour can be modelled by a complex-valued reluctivity tensor (Birkfeld, 1997, 1998). This complex-valued tensor representation is a generalisation of the complex-valued reluctivity scalar used in Lederer and Kost (1998) and Niemenmaa (1988). If ν is considered in its principal coordinate system (Nye, 1985), it is a diagonal tensor whose entries equal ν_{rd} and ν_{td}, respectively[1]. Hence:

$$\begin{pmatrix} \tilde{H}_{rd} \\ \tilde{H}_{td} \end{pmatrix} = \begin{pmatrix} \nu_{rd} & 0 \\ 0 & \nu_{td} \end{pmatrix} \begin{pmatrix} \tilde{B}_{rd} \\ \tilde{B}_{td} \end{pmatrix}, \tag{6}$$

with $\vec{\tilde{H}} = \tilde{H}_{rd}\vec{e}_{rd} + \tilde{H}_{td}\vec{e}_{td}$ the field strength [A/m] and $\vec{\tilde{B}} = \tilde{B}_{rd}\vec{e}_{rd} + \tilde{B}_{td}\vec{e}_{td}$ the flux density [Vs/m^2]. Since the x and y components of $\vec{\tilde{H}}$ and $\vec{\tilde{B}}$ are phasors, $\vec{H}(t)$ and $\vec{B}(t)$ describe an elliptical locus in space.

2.1 Polar tensor representation

By representing the tensor entries in a polar form, i.e.

$$\nu_{rd} = |\nu_{rd}|e^{j\alpha_{rd}}, \tag{7}$$

$$\nu_{td} = |\nu_{td}|e^{j\alpha_{td}}, \tag{8}$$

it follows that

$$\nu = \begin{pmatrix} |\nu_{rd}| & 0 \\ 0 & |\nu_{td}| \end{pmatrix} \begin{pmatrix} e^{j\alpha_{rd}} & 0 \\ 0 & e^{j\alpha_{td}} \end{pmatrix}. \tag{9}$$

The moduli $|\nu_{rd}|$ and $|\nu_{td}|$ basically determine the anisotropic behaviour, while the arguments α_{rd} and α_{td} yield a phase lag between the field and the flux density. To illustrate the meaning of this, a rotating flux density, e.g.

$$\tilde{B}_{rd} = B, \tag{10}$$

$$\tilde{B}_{td} = -jB, \tag{11}$$

is applied to a linear anisotropic material for which $|\nu_{td}| = 4|\nu_{rd}|$. The field strength locus,

$$\vec{H}(t) = \Re\{\vec{\nu}\vec{B}e^{j\omega t}\}, \tag{12}$$

is shown in Figure 1. The instantaneous geometric angle $\delta(t)$ between $\vec{H}(t)$ and $\vec{B}(t)$ is shown in Figure 2. These figures reveal some important properties:

- if $\alpha_{rd} = \alpha_{td}$, the $\vec{H}$-locus is not oblique (Figure 1);
- in general, $\vec{B}$ and $\vec{H}$ are not parallel to each other, except when $\vec{B}$ aligns with one of the principal axes of the $\vec{H}$-locus (Figure 1);
- if $\alpha_{rd} = \alpha_{td} = \alpha$, the direction of $\vec{H}$ depends on the value of α (Figure 1); and
- if $\alpha_{rd} = \alpha_{td} = 0$, the average value of $\delta(t)$ is zero. The total loss

$$P_h = \int_{\omega t=0}^{2\pi} \vec{H}\,d\vec{B} = \int_{\omega t=0}^{2\pi} H_x\,dB_x + \int_{\omega t=0}^{2\pi} H_y\,dB_y \tag{13}$$

is zero as well (Figure 2).

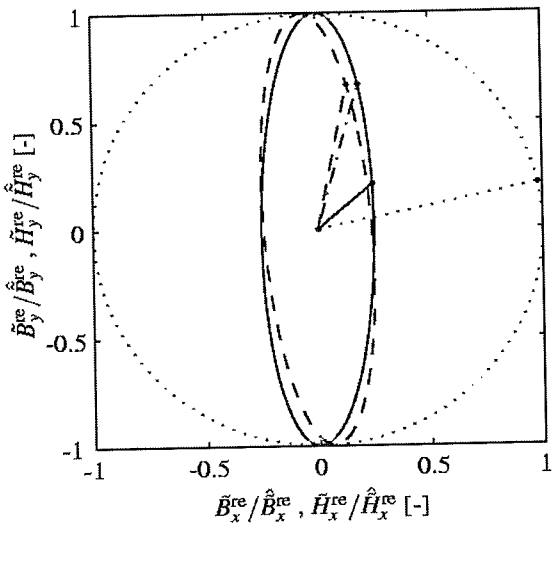

Figure 1.
Elliptical $\vec{H}$-loci obtained when applying a circular $\vec{B}$-locus to a linear anisotropic material, represented by a complex reluctivity tensor for which $|\nu_{td}|=4\,|\nu_{rd}|$, $\alpha_{rd}=\alpha_{td}=0°$ (solid), $\alpha_{rd}=\alpha_{td}=30°$ (dashdotted), $\alpha_{rd}=45°$ and $\alpha_{td}=30°$ (dashed)

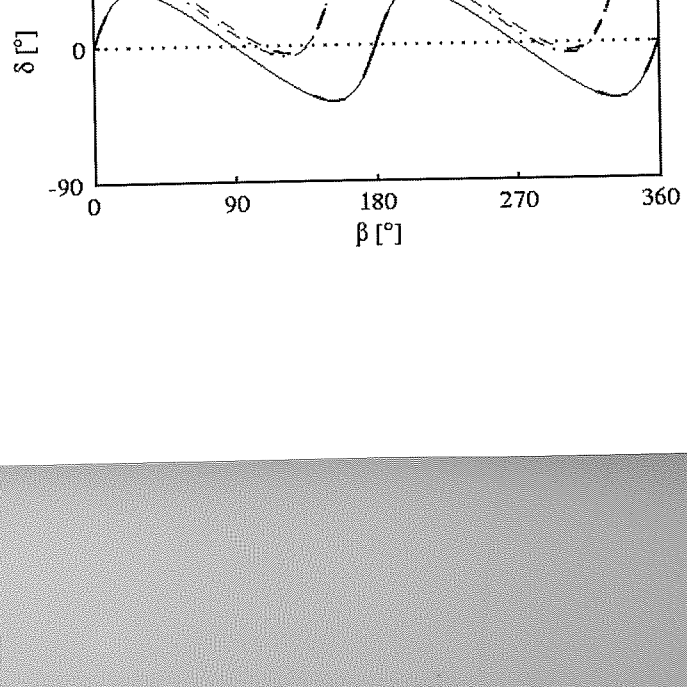

Figure 2.
Geometrical angle ($\delta(t)$ between $\vec{H}(t)$ and $\vec{B}(t)$, when applying a circular $\vec{B}$-locus to a linear anisotropic material, represented by a complex reluctivity tensor for which $|\nu_{td}|=4|\nu_{rd}|$, $\alpha_{rd}=\alpha_{td}=0°$ (solid), $\alpha_{rd}=\alpha_{td}=30°$ (dashdotted), $\alpha_{rd}=45°$ and $\alpha_{td}=30°$ (dashed)

- If $\alpha_{rd} = \alpha_{td} \in]0°, 180°[$ or $\alpha_{rd} \neq \alpha_{td} \in [0°, 180°]$, the average value of $\delta(t)$ is positive, resulting in a positive total loss (Figure 2).

As a consequence, a complex-valued reluctivity tensor allows to model the losses caused by simultaneously alternating and rotating fluxes, though in a simplified way (Birkfeld, 1998). If $|\nu_{rd}| = |\nu_{td}|$ and $\alpha_{rd} = \alpha_{td} \in [0°, 180°]$, the reluctivity tensor may be replaced by a complex-valued scalar reluctivity, which models a simplified form of alternating hysteresis (Lederer and Kost, 1998).

2.2 Cartesian tensor representation

By representing the reluctivity tensor components in cartesian form, i.e.

$$\nu_{rd} = \nu_{rd}^{re} + j\nu_{rd}^{im}, \tag{14}$$

$$\nu_{td} = \nu_{td}^{re} + j\nu_{td}^{im}, \tag{15}$$

it follows that:

$$\nu = \begin{pmatrix} \nu_{rd}^{re} & 0 \\ 0 & \nu_{td}^{re} \end{pmatrix} + j \begin{pmatrix} \nu_{rd}^{im} & 0 \\ 0 & \nu_{td}^{im} \end{pmatrix}. \tag{16}$$

Since $\mathbf{K}$ depends on ν, the entries of $\mathbf{K}$ may be complex-valued. By splitting up $\mathbf{K}$ in its real and imaginary part,

$$\mathbf{K} = \mathbf{K}^{re} + j\mathbf{K}^{im}, \tag{17}$$

the system of equation (5) becomes

$$\tilde{\mathbf{r}}(\tilde{\mathbf{A}}) = [\mathbf{K}^{re}(\tilde{\mathbf{A}}) + j(\mathbf{L} + \mathbf{K}^{im}(\tilde{\mathbf{A}}))]\tilde{\mathbf{A}} - \tilde{\mathbf{T}} = \mathbf{0}. \tag{18}$$

2.3 Material data

Birkfeld (1998), described how ν_{rd}^{re}, ν_{rd}^{im}, ν_{td}^{re} and ν_{td}^{im} can be determined from measurements in the rolling and transverse direction of grain-oriented silicon steels, by processing the measured signals in frequency domain. Obviously, the results depend on the shape of the exciting $\vec{B}$-locus.

For a circular $\vec{B}$-locus, these reluctivity tensor components are shown in Figure 3 as a function of the magnitude of $\vec{B}$. The measurements have been performed at 50 Hz on a square grain-oriented silicon steel sheet M111-35N of 80 mm length and 0.35 mm thickness (Beckley, 2000). For ease of notation, $\nu_{rd}^{re,im}$ denotes both ν_{rd}^{re} and ν_{rd}^{im}. The solid and dashed lines correspond to the real and imaginary tensor component, respectively.

The polar equivalent of this figure, describing the dependency of $|\nu_{rd}|$, $|\nu_{td}|$, α_{rd} and α_{td} on $|\vec{B}|_{max}$, is shown in Figure 4. Here, the solid and dashed lines correspond to the rolling and transverse direction, respectively. The moduli in this figure reveal the obvious result that the rolling direction is easier to magnetise than the transverse direction. Moreover, the elliptic $\vec{H}$-locus has its principal axes close to the rolling and transverse direction, because $\alpha_{rd} \approx \alpha_{td}$. The fact that they both differ from zero implies that the material is not lossless.

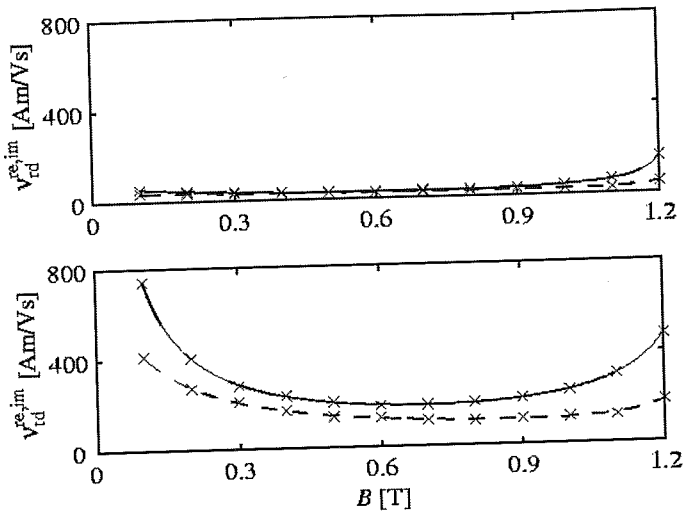

Figure 3.
Reluctivity tensor entries ν_{rd}^{re} (top, solid), ν_{rd}^{im} (top, dashed), ν_{td}^{re} (bottom, solid) and ν_{td}^{im} (bottom, dashed) as a function of the magnitude B of a circular flux density (Birkfeld, 1998)

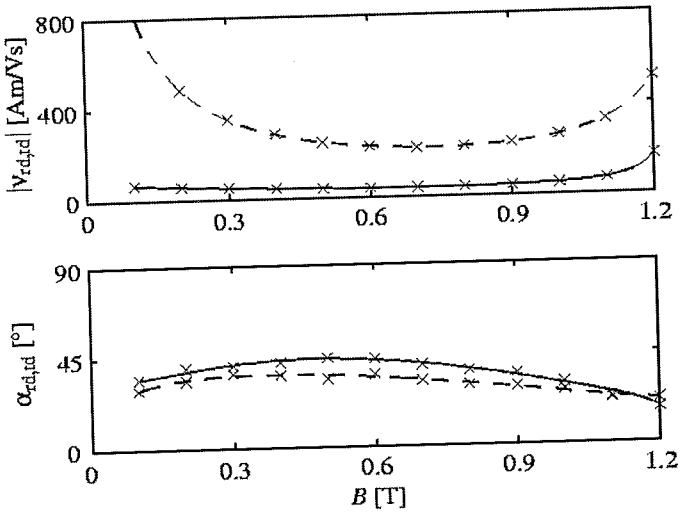

Figure 4.
Reluctivity tensor entries $|\nu_{rd}|$ (top, solid), $|\nu_{td}|$ (top, dashed), α_{rd} (bottom, solid) and α_{td} (bottom, dashed) as a function of the magnitude B of a circular flux density (Birkfeld, 1998)

3. Newton-Raphson method

It is possible to solve equation (18) numerically by successive substitution. The conjugate orthogonal conjugate gradient (COCG) method can be used for this purpose, since the complex-valued system is symmetric. Simulation time can be significantly decreased by considering derivative information of the reluctivity tensor entries as well, to yield the Newton-Raphson method. However, this requires a special treatment. The basic idea behind the Newton-Raphson algorithm is to set the first-order Taylor series expansion of the residual $\tilde{\mathbf{r}}(\tilde{\mathbf{A}})$ to zero. However, when working with complex

variables, the Taylor series expansion is only defined if the residual is an analytic function of $\tilde{\mathbf{A}}$, i.e. the Cauchy-Riemann condition

$$\frac{\partial \tilde{\mathbf{r}}}{\partial \tilde{\mathbf{A}}_k^{re}} = \frac{1}{j} \frac{\partial \tilde{\mathbf{r}}}{\partial \tilde{\mathbf{A}}_k^{im}} \tag{19}$$

must be fulfilled. Unfortunately, in non-linear magnetodynamic problems, this is generally not the case (Lederer *et al.*, 1996).

Consequently, in order to obtain a Newton-Raphson scheme, one has to derive the Jacobian from the equivalent real representation of $\tilde{\mathbf{r}}$, defined by

$$\mathbf{r} = \begin{pmatrix} \tilde{\mathbf{r}}^{re} \\ \tilde{\mathbf{r}}^{im} \end{pmatrix}. \tag{20}$$

By setting

$$\mathbf{D} = \begin{pmatrix} \mathbf{K}^{re} & -(\mathbf{L} + \mathbf{K}^{im}) \\ \mathbf{L} + \mathbf{K}^{im} & \mathbf{K}^{re} \end{pmatrix}, \tag{21}$$

$$\mathbf{A} = \begin{pmatrix} \tilde{\mathbf{A}}^{re} \\ \tilde{\mathbf{A}}^{im} \end{pmatrix}, \tag{22}$$

$$\mathbf{T} = \begin{pmatrix} \tilde{\mathbf{T}}^{re} \\ \tilde{\mathbf{T}}^{im} \end{pmatrix}, \tag{23}$$

it follows that

$$\mathbf{r}(\mathbf{A}) = \mathbf{D}(\mathbf{A})\mathbf{A} - \mathbf{T}. \tag{24}$$

The $(2n \times 2n)$ matrix $\mathbf{D}$ has real-valued entries, but it is non-symmetric. The $(2n \times 1)$ vectors $\mathbf{r}$, $\mathbf{A}$ and $\mathbf{T}$ have real-valued entries. Setting the first-order Taylor expansion of $\mathbf{r}$ to zero,

$$\mathbf{r}(\mathbf{A} + \mathbf{d}) \approx \mathbf{r}(\mathbf{A}) + \mathbf{J}(\mathbf{A})\mathbf{d} = 0, \tag{25}$$

with $\mathbf{J}$ the Jacobian of $\mathbf{r}$, yields a direction $\mathbf{r}$ along which a line search is performed in order to determine a new approximation. Elaborating $\mathbf{J}$ on the level of a single linear finite element yields

$$\mathbf{J}^{(e)} = \mathbf{D}^{(e)} + \mathbf{M}^{(e)} + \mathbf{N}^{(e)}, \tag{26}$$

with

$$\mathbf{M}^{(e)} = \frac{2}{\Delta} \mathbf{Q}^{(e)} \begin{pmatrix} \tilde{\mathbf{A}}^{re,(e)} \\ \tilde{\mathbf{A}}^{im,(e)} \end{pmatrix} \begin{pmatrix} \tilde{\mathbf{A}}^{re,(e)} \\ \tilde{\mathbf{A}}^{im,(e)} \end{pmatrix}^{T} \mathbf{P}^{(e)} \tag{27}$$

$$\mathbf{N}^{(e)} = \frac{2}{\Delta}\mathbf{R}^{(e)}\begin{pmatrix} -\tilde{\mathbf{A}}^{\mathrm{im},(e)} \\ \tilde{\mathbf{A}}^{\mathrm{re},(e)} \end{pmatrix}\begin{pmatrix} \tilde{\mathbf{A}}^{\mathrm{re},(e)} \\ \tilde{\mathbf{A}}^{\mathrm{im},(e)} \end{pmatrix}^{\mathrm{T}}\mathbf{P}^{(e)} \tag{28}$$

$$\mathbf{P}_{ij}^{(e)} = \frac{1}{4\Delta}\begin{pmatrix} b_i & c_i \end{pmatrix}\begin{pmatrix} b_j \\ c_j \end{pmatrix}, \tag{29}$$

$$\mathbf{Q}_{ij}^{(e)} = \frac{1}{4\Delta}\begin{pmatrix} b_i & c_i \end{pmatrix}\frac{\mathrm{d}\nu'\mathrm{re}}{\mathrm{d}B^2}\begin{pmatrix} b_j \\ c_j \end{pmatrix}, \tag{30}$$

$$\mathbf{R}_{ij}^{(e)} = \frac{1}{4\Delta}\begin{pmatrix} b_i & c_i \end{pmatrix}\frac{\mathrm{d}\nu'\mathrm{im}}{\mathrm{d}B^2}\begin{pmatrix} b_j \\ c_j \end{pmatrix}, \tag{31}$$

where Δ is the area of the element, $b_1 = y_2 - y_3, \ldots$, $c_1 = x_3 - x_2, \ldots$. Due to the non-symmetric structure of the Jacobian, the conjugate gradient (CG) method cannot be used to solve equation (25). The quasi minimal residual (QMR) method is appropriate here. Equating $\mathbf{M}^{(e)}$ and $\mathbf{N}^{(e)}$ in equation (26) to zero, i.e. omitting all non-linear contributions to the Jacobian, gives rise to the Picard or successive substitution method discussed earlier.

4. Simulation of a three-phase transformer

The 3-phase transformer shown in Figure 5 is now simulated using the complex-valued tensor data shown in Figure 3. The phase of the currents in the coils is $-85°$, 35° and 155°, respectively. For three different flux density levels, Figure 6 compares the convergence of the proposed Newton-Raphson method (solid) with the convergence of the Picard or successive substitution method (dashdotted). Obviously, the Newton-Raphson method converges much faster than the Picard method, except if the applied currents are small. This is caused by the negative derivatives of the reluctivity tensor entries at low flux densities shown in Figure 3 (Rayleigh region).

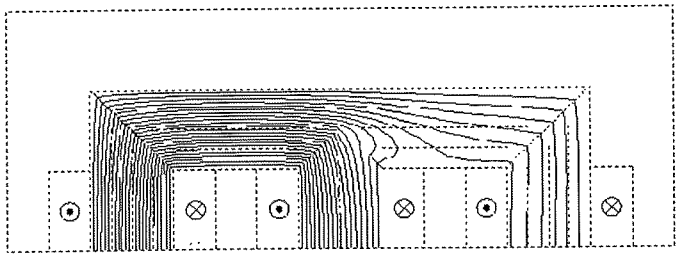

Figure 5.
Flux line distributions obtained with the complex-valued time-harmonic anisotropy model

Notes: The phase of the currents in the coils is –85°, 35° and 155° respectively. The flux density in the middle limb is approximately alternating with an amplitude of 1.17 T

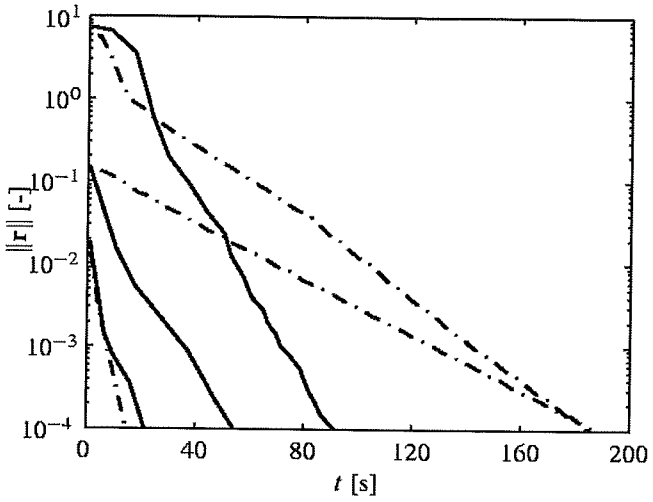

Figure 6.
Norm of the residual as a function of time, for three different flux density levels, when simulating with the Newton-Raphson method (solid) or the Picard method (dashdotted)

Figure 5 shows the flux line distribution. Since the material model used for this simulation assumes that all $\vec{B}$-loci are circular, it is expected that the obtained solution may differ significantly from reality. Data are required for elliptic $\vec{B}$-loci as well, in order to perform more accurate simulation. The use of a complex reluctivity tensor allows to visualise the loss density in each finite element. This is shown in Figure 7 for the region around the T-joint. This figure clearly indicates the increased losses due to rotational magnetisation at the top of the vertical limb.

5. Conclusions

The use of a complex-valued reluctivity tensor allows to model non-linear, anisotropic and hysteretic materials in a time-harmonic context. The equations for solving such type of problems with the Newton-Raphson method are elaborated. The convergence

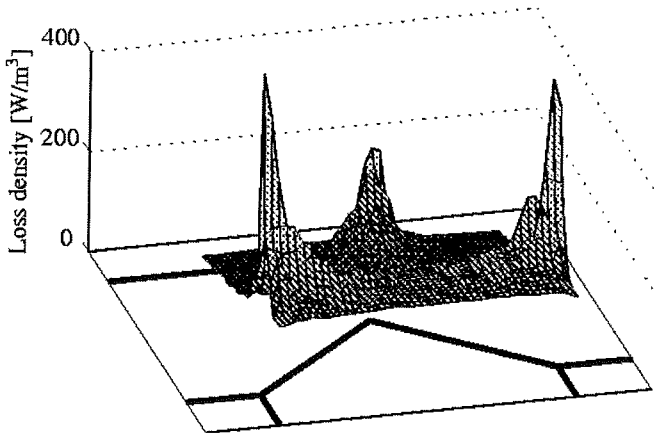

Figure 7.
Loss density distribution in the T-joint of the middle limb

rate for the Newton-Raphson method is significantly higher than for the successive substitution method, provided the simulation is performed outside the Rayleigh region of the material characteristics.

Note

1. "rd" and "td", respectively, stand for "rolling" and "transverse direction", since these directions generally coincide with the principal tensor axes.

References

Birkfeld, M. (1998), "Investigation of the permeability tensor of electrical steel sheet", *IEEE Transactions on Magnetics*, Vol. 34 No. 5, pp. 3667-73.

Birkfeld, M. and Hempel, K.A. (1997), "Calculation of the magnetic behaviour of electrical steel sheet under two-dimensional excitation by means of the reluctance tensor", *IEEE Transactions on Magnetics*, Vol. 33 No. 5, pp. 3757-9.

Beckley, P. (2000), *Electrical Steels*, European Electrical Steels, Newport.

Lederer, D. and Kost, A. (1998), "Modelling of non-linear magnetic material using a complex effective reluctivity", *IEEE Transactions on Magnetics*, Vol. 34 No. 5, pp. 3060-3.

Lederer, D., Igarashi, H. and Kost, A. (1996), "The Newton-Raphson method for complex equation systems", *Proceedings of the 7th International IGTE Symposium on Numerical Field Calculation in Electrical Engineering (IGTE'96), Graz, Austria*, pp. 391-4.

Niemenmaa, A. (1988), "Complex reluctivity modelling of iron losses in induction machines", *Proceedings of the International Conference on Electrical Machines (ICEM'88)*, pp. 633-6.

Nye, J.F. (1985), *Physical Properties of Crystals*, 2nd ed., Oxford Science Publications, Clarendon Press, Oxford.

The Emerald Research R
www.emeraldinsight.c

Comple
finite el
incl
Ji

Department

Electrical

Department of El

Keywords *Finite elem*

Abstract *This paper two-dimensional (2D) fi vectorized Jiles-Atherton and magnetomotive fo Newton-Raphson meth tensor. The proposed m T-joint of a three-phase*

Introduction

In the domain of nu finite element (FE) fi Dupré *et al.*, 1998; S Jiles-Atherton hyster models displaying u 1999). In application vector hysteresis mo are iteratively solved 1999) or the Newton 1999). The latter m solution), but is som

For 2D magnetic potential formulation non-zero component implement. The scal

The research was carr fundamental research Associate with the Bel